Cooperative Light Scattering from θ-Pinch Plasmas*

MARK DAEHLER AND F. L. RIBE

Los Alamos Scientific Laboratory, University of California, Los Alamos, New Mexico

(Received 3 April 1967)

Results are reported of an experiment to measure the cooperative scattering from density fluctuations in the plasma of a 150-kJ, high-voltage θ pinch with a low-pressure (20 mTorr) filling of deuterium gas. The beam from a giant-pulse ruby laser is focused at the center of the plasma, and the light emerging at angles between 5.5° and 7° to the beam and plasma axis is collected and spectrally resolved by a spectrometer consisting of an interference filter and two identical Fabry-Perot interferometers in series. The θ-pinch plasma parameters, separately measured in another experiment, are plasma density $n=2.8\times10^{16}$ cm^{-3}, $kT_e=345$ eV, and $kT_i=2.0$ keV, corresponding to Salpeter's parameters $\alpha=1.2$, $\beta=0.33$. Scattered spectra are reduced to absolute values of $nd^2\sigma/d\Omega d\lambda$ by calibration against Rayleigh scattering from dry N_2 gas. The results show a narrow central peak superimposed on a broader tail of lower magnitude. In the case of no bias field ($B_0=0$), the tail has a width and magnitude equal within experimental error to those of the theoretical thermal-ion feature, corresponding to Doppler broadening of the scattered light by an amount characteristic of the thermal-ion motion at $kT_i=2$ keV. The central peak has a maximum magnitude 15 times greater than that of the theoretical ion feature, and is 0.44 times as wide. For $B_0=-750$ G, the central peak increases in intensity by another factor of 3, while retaining approximately the same width. The central peak is attributed to superthermal-plasma density fluctuations, superimposed on the background represented by the broader thermal-ion feature.

I. THEORETICAL CONSIDERATIONS

A. Spectral Doppler Widths from Light Scattering

THE object of the experiments reported here was to measure the scattering of ruby-laser light from a θ-pinch plasma whose main parameters (size, density n, electron and ion temperatures T_e and T_i) are fairly well known, in order to make further measurements of the plasma properties. The basic process is Thomson scattering of light of incident wave vector $\mathbf{k}_0$ through a small angle θ_s to give scattered wave vector $\mathbf{k}_s$. Because of the motion of the plasma electrons, the scattered light is Doppler shifted, giving a frequency shift $\Delta\omega$ away from the incident frequency ω_0 which has a maximum[1] when the electron velocity $\mathbf{v}_e$ is parallel to the difference wave vector $\delta\mathbf{k}=\mathbf{k}_s-\mathbf{k}_0$, as shown in Fig. 1. For $k_0\approx k_s$ the frequency shift and electron velocity are related by the expression

$$\Delta\omega=|\delta\mathbf{k}|\,v_e=2k_0v_e\sin(\tfrac{1}{2}\theta_s). \tag{1}$$

We are primarily interested in the case of cooperative scattering from a plasma, first observed in the ionosphere,[2,3] rather than scattering from independent plasma electrons. As is well known,[1,4–7] the occurrence of cooperative effects depends on the relationship of $|\delta\mathbf{k}|$ to the electron Debye length

$$\lambda_D=(kT_e/4\pi ne^2)^{1/2}, \tag{2}$$

and they are observable when the quantity

$$\alpha=1/(\lambda_D\,|\,\delta\mathbf{k}\,|) \tag{3}$$

is greater than or equal to unity. The electrons then move cooperatively, as though tied to the ions over regions of size λ_D,[6] and the scattering is determined by plasma density fluctuations whose wave number is $|\delta\mathbf{k}|$. The Doppler broadening or shifting of the scattered light arises from fluctuations having phase velocities $\mathbf{v}_c$ parallel to $\delta\mathbf{k}$. In the present experi-

FIG. 1. Diagram of incident and scattered wave vectors, illustrating mathematical quantities used in the text.
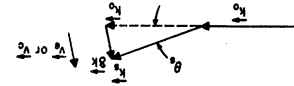
ments, for which θ_s is small and $\mathbf{k}_0$ is parallel to the axis of the discharge, the Doppler broadening therefore measures plasma velocities which are almost transverse to the axis.

B. Scattering from Plasmas in Thermal Equilibrium

Salpeter[5] has calculated the scattering from density fluctuations in a plasma which is in thermal equilibrium, except that T_e and T_i may be different. The spectral distribution of the scattered power is proportional to the following function:

$$df/d\omega=\omega_e^{-1}\Gamma_\alpha(\Delta\omega/\omega_e)+Z\omega_i^{-1}[\alpha^2/(1+\alpha^2)]^2\Gamma_\beta(\Delta\omega/\omega_i). \tag{4}$$

[The functions Γ_α and Γ_β are defined in Eq. (35) of Ref. 5.] The first term represents scattering with a spectral width[8]

$$\omega_e=|\delta\mathbf{k}|\,(2kT_e/m_e)^{1/2}, \tag{5}$$

* Work performed under the auspices of the U.S. Atomic Energy Commission.

[1] J. A. Fejer, Can. J. Phys. **38**, 1114 (1960).
[2] K. L. Bowles, Phys. Rev. Letters **1**, 454 (1958); J. Res. Natl. Bur. Std. (U.S.) **650**, 1 (1961).
[3] V. L. Pineo, L. G. Kraft, and H. W. Briscoe, J. Geophys. Res. **65**, 1620 (1960).
[4] J. Dougherty and D. Farley, Proc. Roy. Soc. (London) **A259**, 79 (1960).
[5] E. E. Salpeter, Phys. Rev. **120**, 1528 (1960).
[6] M. N. Rosenbluth and N. Rostoker, Phys. Fluids **5**, 776 (1962).
[7] D. F. DuBois and V. Gilinsky, Phys. Rev. **133**, A1308 (1964).

[8] The quantity k in association with T_e or T_i is Boltzmann's constant.
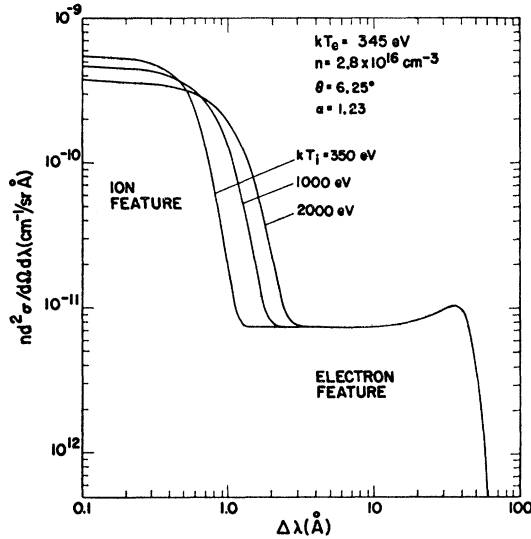
FIG. 2. Computed theoretical scattering spectra for the Scylla III plasma parameters, assuming three values of T_i.

given by the electron thermal broadening, and the second term, the "ion feature," has a width

$$\omega_i = |\delta k| (2kT_i/m_i)^{1/2}, \qquad (6)$$

given by the ion thermal motion. The parameter

$$\beta = [ZT_e\alpha^2/T_i(1+\alpha^2)]^{1/2} \qquad (7)$$

(depending also on the ion charge Z) determines the shape of the ion-feature spectrum.

For $\alpha \ll 1$ the spectrum reduces to that from free electrons and has only the Γ_α contribution, which becomes a Gaussian of width ω_e. For $\alpha \geq 1$ the Γ_α spectrum has two peaks (the "electron satellites") at frequencies given by the dispersion relation for longitudinal electron plasma waves:

$$\Delta\omega_{0e} = \pm[\omega_{pe}^2 + |\delta k|^2 3kT_e/m_e]^{1/2}, \qquad (8)$$

where $\omega_{pe} = (4\pi n e^2/m_e)^{1/2}$ is the electron plasma frequency.

Of more interest in the present experiment is the Γ_β term, which is much more intense than the Γ_α term, since its spectral width is of order ω_i, even though the strengths of the two terms integrated over $\Delta\omega$ are about equal. For $T_i/T_e \gtrsim 1$, the Γ_β spectrum is approximately Gaussian with width ω_i. For $T_i/T_e \ll 1$ two peaks appear at frequency shifts given by the dispersion relation for ion-acoustic waves:

$$\Delta\omega_{0i} = \pm[\omega_{pi}^2 + |\delta k|^2 3kT_e/m_i]^{1/2}, \qquad (9)$$

where $\omega_{pi} = (4\pi n e^2/m_i)^{1/2}$. Graphs of the Salpeter theory are given by Gerry and Patrick.[9] The scattered spectra may be appreciably modified from the Salpeter predictions when the number $(\frac{4}{3})\pi n\lambda_D^3$ of particles in a Debye sphere becomes less than unity.[5,10]

[9] E. T. Gerry and R. M. Patrick, Phys. Fluids **8**, 208 (1965).
[10] O. Theimer, Phys. Letters **20**, 639 (1966).

The theoretical ion feature provides a reference of scattered intensity, which will be referred to hereafter as that due to thermal plasma fluctuations. The spectra shown in Fig. 2 were calculated from an exact expression for the scattered intensity[11] for the parameters of the θ pinch used in the present experiments (cf. Sec. III A), but various values of T_i were assumed. Here we have plotted n times the differential cross section $d^2\sigma/d\Omega d\lambda$, per unit solid angle and per unit of the vacuum wavelength change $\Delta\lambda = -(2\pi/k_0\omega_0)\Delta\omega$. This practice will be adhered to in presenting the data.

The total scattered intensity, integrated over $\Delta\omega$, is proportional to $\langle |\delta n(k)|^2 \rangle$, the time average of the square of the Fourier component of density fluctuations about the average value n, which has wave number $k = |\delta k|$. For a total number N_e of scattering electrons and for $T_e = T_i$, the mean-squared thermal fluctuation is given by

$$\frac{\langle |\delta n(k)|^2 \rangle}{n^2} = N_e^{-1}\frac{1+Z\alpha^2}{1+(Z+1)\alpha^2}. \qquad (10)$$

Except for the function of order unity on the right, which expresses the two-electron correlation, this is of order N_e^{-1}, the fluctuation to be expected for randomly distributed electrons. For $T_e \neq T_i$ the function on the right is somewhat different.[11]

C. Nonequilibrium Plasmas

Little has been done to calculate scattering from nonequilibrium plasmas. For $\alpha > 1$, $T_e \geq T_i$ Rosenbluth and Rostoker[6] have calculated the spectrum of density fluctuations for a net electron drift velocity v_D relative to the ions, in which case the ion-acoustic waves become unstable. As this situation is approached, the spectral intensity increases by more than an order of magnitude over the thermal level. In interpreting the measurements reported here, we adopt the view, guided by this example, that scattered intensities much greater than the thermal levels of Fig. 2 represent collective plasma density fluctuations superimposed on the thermal background.

II. PREVIOUS SCATTERING EXPERIMENTS ON LABORATORY PLASMAS

In laser-beam scattering experiments use has been made of the plasmas of arcs[12–14] and a sheet triaxial pinch,[15] as well as various types of θ pinches. Of the θ-pinch measurements, many have been performed on

[11] W. Kegel, Institute für Plasmaphysik Report No. IPP6/21 1964 (unpublished). We are indebted to F. C. Jahoda for providing a computer code to calculate the scattering spectra of Fig. 2. to F. C. Jahoda for providing a computer code to calculate the scattering spectra of Fig. 2.
[12] A. W. de Silva, D. E. Evans, and M. J. Forrest, Nature **203**, 1321 (1964).
[13] E. T. Gerry and D. J. Rose, J. Appl. Phys. **37**, 2715 (1966).
[14] P. W. Chan and R. A. Nodwell, Phys. Rev. Letters **16**, 122 (1966).
[15] O. A. Anderson, Phys. Rev. Letters **16**, 978 (1966).

small devices,[16–22] comparable in energy and plasma properties to the preionizer used in the present experiment. Medium-energy θ pinches,[23–26] with energies $\frac{1}{6}$ to $\frac{1}{4}$ that of the present experiment have also recently been used, as well as one of comparable energy,[27] and a much larger device[28] (which has, however, not been used for cooperative scattering measurements).

Except in those cases where the θ pinch was used to produce an afterglow plasma,[19,20,22] and the very large device, all previous θ-pinch scattering experiments have made use of the "high-pressure" regime of operation. In this regime the hydrogen filling pressure is of the order of 0.1 Torr, and the ion energy is derived mainly from the annihilation of an antiparallel bias field B_0 of the order of a few kG.[29,30] The Scylla III device of the present experiments, on the other hand, was operated in the low-pressure regime[31–33] (filling pressure of the order of 0.01 Torr), where considerably higher ion energies are produced without benefit of B_0.

There is little doubt of the applicability of small-α, large-angle scattering measurements of the electron feature to determine plasma temperature and density.[12,13,18–20,22,23,28] Measurements at $\alpha \approx 1$ have shown the incipient plasma-frequency satellites,[15,17,18,25] allowing simultaneous determination of kT_e and n from the shape of the electron feature, while forward-scattering measurements[14,20,27] at $\alpha \approx 2$ to 4 have shown well-resolved electron satellites.

The narrow ion feature has been observed[12,17,20,21] and resolved.[15,23,26,27] In the case of the triaxial pinch measurement,[15] the value of kT_i derived from the width of the ion feature in the dense, cool (2-eV) plasma is equal to kT_e, and its magnitude has the expected theoretical value relative to that of the electron feature. Two of the θ-pinch measurements[23,26] of the ion feature have shown an asymmetric spectrum. However, no comparison of the ion-feature Doppler width with other measurements of kT_i was possible, and its main features could be attributed to nonthermal, ion-acoustic waves, excited by electron drift, as described in Sec. IC. The third θ-pinch measurement[27] gives a symmetric spectrum, and the value of kT_i deduced from D–D neutron-emission rate measurements is in agreement with that corresponding to the width of the ion feature. In the present measurements both the magnitude and spectral shape of the ion feature were determined for a plasma whose properties (particularly kT_i) have been independently measured, allowing a comparison with the theoretical spectrum of scattering to be expected from thermal density fluctuations. It is of particular intrest that the ion temperature (energy) of the present experiments is an order of magnitude larger than that of the previous three measurements. In addition, the measurements are localized to a small region at the center of the plasma, in contrast to the previous measurements, where light was collected from a large portion of the plasma.

III. APPARATUS

A. The θ Pinch

1. Machine Parameters. The θ pinch used in these experiments is a modification of the Scylla III device described earlier,[34,35] and the properties of its plasmas are fairly well known. Whereas the discharge was previously operated in the high-pressure regime (filling pressure of $D_z \approx 90$ mTorr; initial, reversed bias field $B_0 \approx -4$ kG) the present experiments were performed in the low-pressure regime[31–33] with a filling pressure of 20 mTorr and little or no bias field. The θ pinch consists essentially of a single-turn aluminum (compression) coil of 20-cm length and 10-cm av. i.d. with a geometric mirror ratio of 1.48. The 150-kJ capacitor bank (reduced somewhat in voltage and capacitance since the experiments of Refs. 34 and 35) is charged to 76 kV, giving a peak magnetic field of 65 kG with a quarter-cycle (rise) time of 2.5 μsec. The discharge is preionized, so that the hot plasma is produced during the first half-cycle of the magnetic field which is then "crowbarred,"[35] to prevent subsequent reversal.

The plasma properties of the Scylla III θ pinch, as

[16] E. Fünfer, B. Kronast, and H. J. Kunze, Phys. Letters **5**, 125 (1963).

[17] H. J. Kunze, E. Fünfer, B. Kronast, and W. H. Kegel, Phys. Letters **11**, 42 (1964); P. Hubert and E. Crémieu-Alcan, *Comptes Rendus de la IVe Conférence Internationale sur les Phénomènes dans les Gas* (Bureau des Editions, CEN, Saclay), Vol. IV, p. 119.

[18] H. J. Kunze, Z. Naturforsch. **20a**, 801 (1965).

[19] W. E. R. Davies and S. A. Ramsden, Phys. Letters **8**, 179 (1964).

[20] S. A. Ramsden and W. E. R. Davies, Phys. Rev. Letters **16**, 303 (1966).

[21] U. Ascoli-Bartoli, J. Katzenstein, and L. Lovisetto, Nature **204**, 672 (1964); **207**, 63 (1965).

[22] T. Consoli, G. Gormezano, and L. Slama, Phys. Letters **20**, 267 (1966).

[23] B. Kronast, H. Röhr, E. Glock, H. Zwicker, and E. Fünfer, Phys. Rev. Letters **16**, 1082 (1966).

[24] H. J. Kunze, A. Eberhagen, and E. Fünfer, Phys. Letters **13**, 308 (1964).

[25] D. E. Evans, M. J. Forrest, and J. Katzenstein, Nature **211**, 23 (1966).

[26] D. E. Evans, M. J. Forrest, and J. Katzenstein, Nature **212**, 21 (1966).

[27] S. A. Ramsden, R. Benesch, W. E. R. Davies, and P. K. John, IEEE J. Quantum Electron. **QE2**, 267 (1966).

[28] C. Andelfinger, G. Decker, E. Fünfer, A. Heiss, M. Keilhacker, J. Sommer, and M. Ulrich, in *Plasma Physics and Controlled Fusion Research* (International Atomic Energy Agency, Vienna, 1966), Vol. I, p. 249.

[29] A. C. Kolb, C. B. Dobbie, and H. R. Griem, Phys. Rev. Letters **3**, 5 (1959).

[30] E. M. Little, W. E. Quinn, and F. L. Ribe, Phys. Fluids **4**, 711 (1961).

[31] L. M. Goldman, H. C. Pollock, J. A. Reynolds, and W. F. Westendorp, Phys. Rev. Letters **9**, 361 (1962).

[32] L. M. Goldman, R. W. Kilb, H. C. Pollock, and J. A. Reynolds, Phys. Fluids **8**, 522 (1966).

[33] E. M. Little, W. E. Quinn, and G. A. Sawyer, Phys. Fluids **8**, 1168 (1965).

[34] E. M. Little, W. E. Quinn, F. L. Ribe, and G. A. Sawyer, Nucl. Fusion Suppl. **2**, 497 (1962).

[35] E. M. Little and W. E. Quinn, Phys. Fluids **6**, 875 (1963).
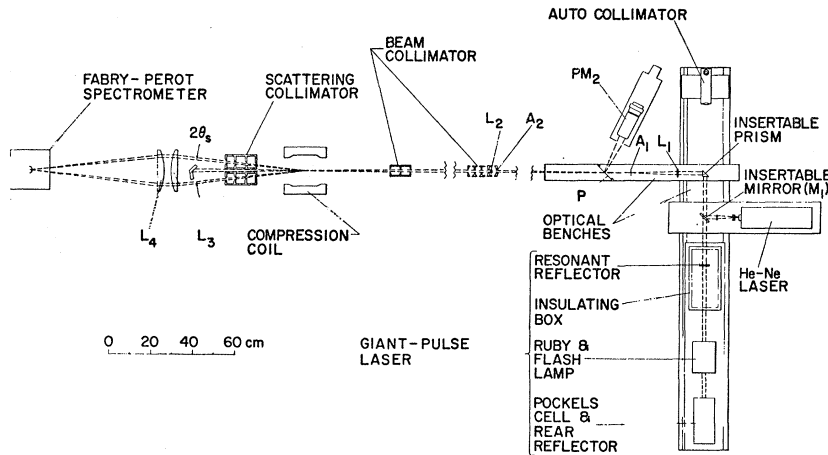
Fig. 3. Schematic plan view, to scale,
of the apparatus.

operated in the present experiment, have recently been extensively remeasured[36]; we briefly summarize them.

2. *Electron Temperature.* Basically, this is determined by measuring the soft x-ray continuous spectrum from the plasma.[37] It was shown in Ref. 34 that spectrometric continuum measurements agree well with absorption measurements, provided that the absorbers used are sufficiently thick to exclude line radiation in the soft x-ray region. The absorber method gives an electron temperature of 345±40 eV for the parameters used in the present experiment.

3. *Plasma Density.* The density of the plasma column was measured absolutely by means of a He-Ne laser interferometer,[38,39] operating at a wavelength of 3.39 μ. The relative radial density distribution, measured by spatially resolving its visible continuum emission, is roughly triangular with a base width of 2.0 cm, and the absolute peak value $n(0)$ is $(2.8\pm0.4)\times10^{16}$ cm^{-3}. The line density N is about 4.6×10^{16} cm^{-1}.

4. *Ion Temperature.* The ion temperature T_i (more properly, the mean ion energy) may be estimated from the neutron yield Y_n, by using the relation

$$Y_n = \tfrac{1}{2}N\bar{n}\langle\sigma v\rangle\tau l, \qquad (11)$$

where $\bar{n}$ is the electron density averaged over plasma radius, τ is the mean time of emission of D–D neutrons, and l is the effective plasma length. The quantity $\langle\sigma v\rangle$ is the Maxwellian average of the neutron branch of the D–D fusion cross section over the relative velocity v of the ions,[40] and is a function of kT_i. Ion temperatures so estimated have previously been found to agree with those determined by Doppler-broadening

measurements[41] and by the measured ratio of the D–He^3 and D–D reaction rates.[42] It has also been found[43] that mean ion energies in the plasma, determined by measuring the energy spectrum of particles escaping out the end of the θ pinch, give neutron yields in good agreement with Eq. (11). Thus, we take neutron yield as one measure of T_i in the present experiment, interpolating a value of $l (\approx 5$ cm) for the present coil length and diameter from measured values in other high-voltage θ pinches.[32,33,41] The value of kT_i corresponding to the average neutron yield for the scattering measurements with no bias field is 2.0±0.1 keV; for the case with small bias field $(B_0 = -750$ G) kT_i is approximately the same, assuming N and $\bar{n}$ to be the same as for $B_0 = 0$.

In the recent Scylla III measurements,[36] kT_i was also determined independently by measuring the ratio of plasma pressure to magnetic pressure electromagnetically. A measurement was made of the magnetic flux excluded by the plasma, as well as the absolute distribution $n(r)$ of density, referred to above, to give the values B $r)$ of magnetic field inside the plasma. Since the external compression field B_e and the value of kT_e are known, the value of kT_i is derived from the pressure balance equation

$$B_e^2/8\pi = B(r)^2/8\pi + n(r)k(T_e + T_i). \qquad (12)$$

The average value thus measured was $kT_i = 2.0$ keV, in good agreement with the neutron-yield value.

B. The Scattering System

The scattering system shown in Fig. 3 consists primarily of the giant-pulse ruby laser, with its beam-defining optics and beam dump; the plasma-producing θ pinch, of which only the compression coil is indicated;

[36] V. A. Finlayson, F. C. Jahoda, G. A. Sawyer, and K. S. Thomas, in Los Alamos Scientific Laboratory Report, No. LA-3628-MS, 1966, p. 25 (unpublished); Phys. Fluids 10, 1564 (1967).

[37] G. A. Sawyer, F. C. Jahoda, F. L. Ribe, and T. F. Stratton, J. Quant. Spectr. Radiative Transfer 2, 467 (1963).

[38] D. E. T. F. Ashby and D. F. Jephcott, Appl. Phys. Letters 3, 13 (1963).

[39] D. A. Baker, J. E. Hammel, and F. C. Jahoda, Rev. Sci. Instr. 36, 395 (1965).

[40] J. L. Tuck, Nucl. Fusion 1, 201 (1961).

[41] D. E. Nagle, W. E. Quinn, F. L. Ribe, and W. B. Riesenfeld, Phys. Rev. 119, 857 (1960).

[42] L. M. Goldman, R. W. Kilb, and H. C. Pollock, Phys. Fluids 7, 1005 (1964).

[43] R. L. Bingham, L. M. Goldman, and R. W. Kilb, in *Plasma Physics and Controlled Nuclear Fusion Research* (International Atomic Energy Agency, Vienna, 1966), Vol. I, p. 301.
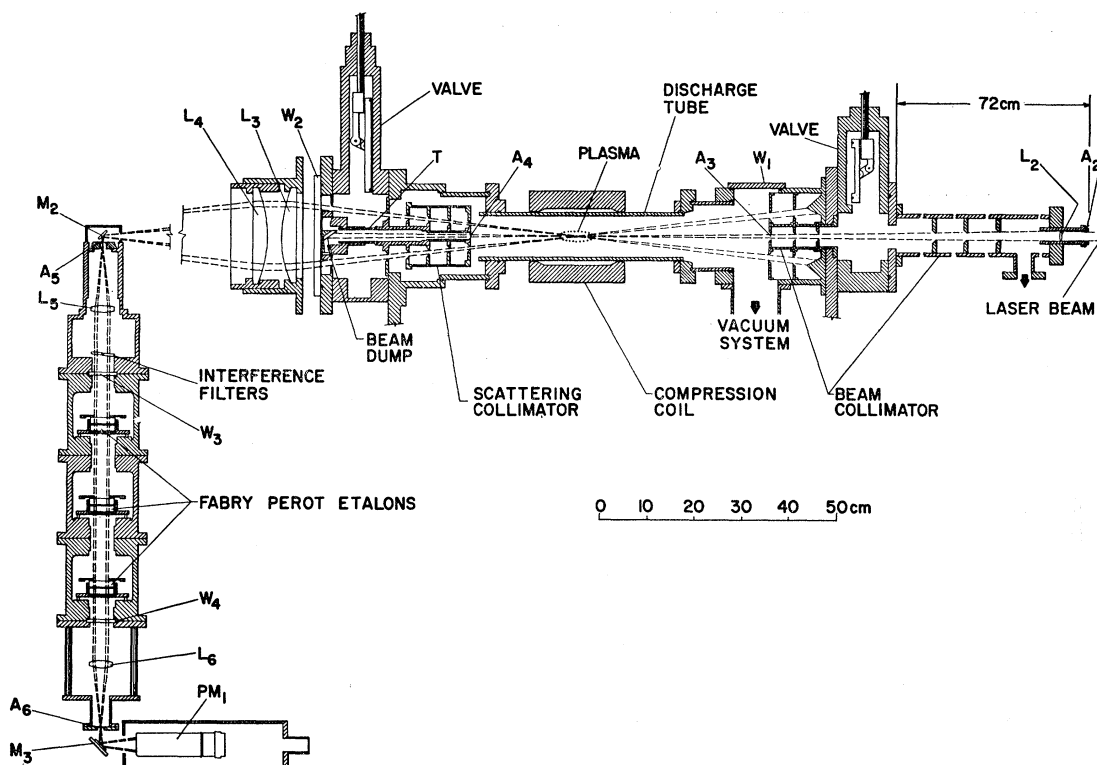
FIG. 4. Side view of the scattering apparatus and Fabry-Perot spectrometer.

the apertures and lenses which define and collect the scattered beam; and the Fabry-Perot spectrometer.

The laser beam is focused by lens L_1, and then refocused onto the center of the plasma by lens L_2, the beam being limited at this lens by aperture A_2 (18-mm diam). The angle φ at L_2 subtended by the 1.5-mm aperture A_1 is 0.0021 rad, so that the etendue[44] of the laser beam is $\pi\varphi^2 A_2 = 9.18 \times 10^{-4}$ mm^2 sr. From the center of the plasma the beam diverges and enters the beam dump, where it is absorbed in two reflections from Corning 5113 glass set at the Brewster angle for zero reflection of the horizontally polarized laser beam. Two sets of baffles, provided to reduce stray light, are illustrated in more detail in Fig. 4.

At the opposite end (Fig. 4) a set of collimating apertures selects light from the center of the plasma scattered into angles from the axis between 5.5° and 7°, the mean scattering angle being $\theta_s = 6.25°$. A pair of lenses L_3 and L_4 gather the scattered light, imaging the primary laser spot from the center of the plasma onto the entrance aperture of the spectrometer with unit magnification. The solid angle of scattered light collected is 0.018 sr.

Alignment of the optical system is facilitated by a CW He-Ne laser (Spectraphysics 130) whose beam is expanded to match the lateral dimensions of the ruby

laser beam. The insertable mirror and insertable prism of Fig. 3 may be removed and reinserted in their exact positions, a convenience making it possible to align the two laser beams exactly together, with respect to both beam direction (using the autocollimating telescope) and lateral positioning. Using the CW laser, the system is carefully aligned so that the beam is centered on the entrance aperture and on aperture A_4 in front of the beam dump. An additional alignment convenience is a piece of ground glass, mounted on a retractable arm, which can be inserted into the center of the discharge tube without breaking the vacuum. The CW-laser light scattered by the ground glass can be seen on the spectrometer aperture, and the spectrometer axis is aligned with this beam.

C. The Laser

The giant-pulse ruby laser, shown at the right in Fig. 3, is the Korad Model K-1Q. Its basic parts include a double sapphire-plate front reflector, a ruby rod 9.5 mm in diam and 15 cm long, and a total-internal-reflection (Porro) prism as the rear reflector. Q switching is accomplished by the half-wavelength Pockels cell. In order to select a single mode, both the ruby and resonant reflector are carefully temperature controlled, as described elsewhere.[45] With these precautions, the

---

[44] The term "etendue" refers to the product of cross sectional area and divergence solid angle of a light beam.

[45] M. Daehler, G. A. Sawyer, and E. L. Zimmermann, J. Appl. Phys. **38**, 1980 (1967).
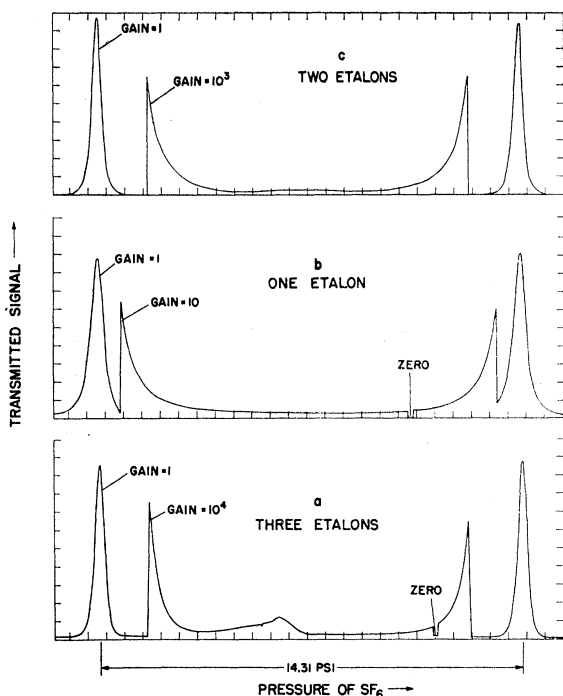
FIG. 5. (a) and (b), transmission curves of the Fabry-Perot spectrometer with one and with three etalons, using CW He-Ne laser light and 0.5-mm apertures; (c) transmission curve with two etalons and 1.5-mm apertures.

laser output consists of a single emission line of 25-nsec duration, with a spectral width less than 0.02 Å and with sidebands having intensities of at most 0.3% of the main component. The peak power is about 75 MW, of which 60% passes through the aperture A_1. The relative intensity of the laser is monitored by a pellicle beam splitter P and the photomultiplier PM_2, as shown in Fig. 3.

D. The Fabry-Perot Spectrometer

The multietalon spectrometer is patterned after the PEPSIOS spectrometer[46] developed by the late J. E. Mack and associates. As shown at the left in Fig. 4, its dispersive elements consist of up to three Fabry-Perot etalons, in a sealed aluminum chamber, and an interference filter. Two lenses and two apertures collimate the light transmitted by the etalons and restrict the range of angles of transmission to 0.011 rad, so that the RCA-7265 photomultiplier PM_1 detects only the central spot of the Fabry-Perot fringe pattern. The interference filter, whose full width at half-maximum (FWHM) is 5.1 Å, transmits only one order of the fringe system.

The Fabry-Perot plates[47] are of fused silica, with a flatness approaching $\lambda/200$, coated with dielectric multilayers of 95% reflectivity at 6943 Å. Unlike the vernier spacer ratios of the PEPSIOS spectrometer, the

[46] J. E. Mack, D. P. McNutt, F. L. Roesler, and R. Chabbal, Appl. Opt. **2**, 873 (1963).
[47] The etalons were obtained from H. W. Yates of Optical Surfaces Ltd., Surrey, England, through Industrial Optics Corporation of Bloomfield, New Jersey.

spacings for these three etalons are identical. The three spacers of each etalon are fused silica discs 6 mm in diam and 0.45 mm thick and are optically contacted to the Fabry-Perot plates. The etalons are adjusted for parallelism by visual observation of the ring pattern, using diffuse neon light. In successive adjustments, the spacing of one etalon can be made identical to that of another to within 1/100 of an order by observing the gas pressure in the spectrometer chamber at which light from a monochromatic source is transmitted.

Scanning is accomplished by changing the pressure of SF_6 in the Fabry–Perot chamber, a 5 Å scanning range requiring a pressure range of 784 Torr at a wavelength of 6943 Å. During the scattering experiment, data were taken "shot by shot," adjusting the SF_6 pressure each time a change in spectrometer wavelength was desired. For measuring the spectrometer characteristics, however, it was more convenient to make continuous scans, with SF_6 leaking into the chamber through a needle valve and illumination by monochromatic (6328 Å) He-Ne laser light scattered by the retractable ground glass in the scattering chamber. Figures 5(a) and 5(b) show the capabilities of the spectrometer, using 0.5-mm-diam apertures. A single etalon shows a finesse (ratio of free spectral range to transmittance band width) of about 35 and a contrast (peak-to-minimum transmittance ratio) of 360. For three etalons the finesse is 45 and the contrast is 1.2×10^6.

The basic reason for using more than one etalon is to take advantage of the increased contrast. For all of the data reported here, two etalons were used, for which a contrast of about 45 000 and a finesse of 40 were measured [Fig. 5(c)]. In the experiment this allowed the weak scattering tail at large $\Delta\lambda$ to be measured in the presence of the strong central feature near $\Delta\lambda = 0$. At the longer wavelength of the ruby laser, the finesse is somewhat increased because the dielectric coatings have higher reflectivity; with two etalons, the finesse was measured to be 44. The dispersion of the spectrometer at λ 6943 was determined by measuring the plate spacing (0.4542±0.0005 mm) and the SF_6 pressure difference between orders (16.90 psi); it is 0.3296± 0.0005 Å/psi.

Since the interference filter transmittance is not constant over the entire scanning range, it was necessary to make a correction to the data, amounting to a few percent typically, but for a few points on the tail of the spectrum as much as 45%. For some data on the wings of the measured spectra the filter was tilted to give higher transmittance. For all filter angles used, the filter transmittance was carefully measured, using a parallel white-light source and a Jarrell-Ash half-meter grating spectrometer.

IV. DATA AND RESULTS

A. The Plasma-Scattering Measurements

The method of data taking is illustrated in Fig. 6 by three oscillograms taken for a single plasma discharge

without reversed bias field. The θ-pinch compression field, applied about 13 μsec after the weaker preionizer field, is monitored in the top oscillogram. The giant-pulse laser was triggered slightly before peak compression, as shown in the middle oscillogram. The bottom oscillogram shows the spectrometer scattered-light pulse and the laser intensity monitor pulse. Measurements of the stray light scattered from the apertures or other parts of the discharge chamber were made in the same way, but without the discharge. These measurements also provided a measure of the spectrometer resolution. The scattered-signal magnitudes were divided by the monitor signals and reduced to absolute values of $nd^2\sigma/d\Omega d\lambda$, using the N_2 Rayleigh-scattering calibration derived below. The neutrons produced by the plasma are monitored both by a calibrated silver-covered Geiger-counter arrangement, to determine the absolute neutron flux by the Ag^{110} β decay, and by a plastic scintillation detector to measure the instantaneous rate of emission. The scintillator output, shown in the top oscillogram, indicates the fraction of the total yield which may be attributed to the first half-cycle of the compression field. Data were taken only for those discharges whose Geiger-counter neutron yields were within 14% of the average value.

B. Absolute Calibration of the Scattered Signals

The scattered-signal magnitudes were reduced to absolute values of the density–cross-section product $nd^2\sigma/d\Omega d\lambda$ by a direct comparison with the known Rayleigh scattering from dry nitrogen gas. In this way it was unnecessary to know the scattering volume, the solid angle of the scattered beam, the absolute laser power, and the window and lens transmittances, since these were the same for both plasma and N_2 scattering. The N_2 gas was introduced into the discharge tube through a liquid-N_2 trap and the linear dependence of Rayleigh-scattered signal (normalized to the laser monitor signal) on N_2 pressure was verified. The calibration was performed at the beginning or end of each plasma run, with the exception of the data of Fig. 8(a), where relative data were normalized to absolute peak-value runs made on days immediately before and after.

The Rayleigh differential cross section in the forward direction, perpendicular to the incident polarization direction, is[48]

$$(d\sigma/d\Omega)_R = (16\pi^4/\lambda_0^4)\gamma^2, \qquad (13)$$

where λ_0 is the wavelength of the incident light and γ, the polarizability of the N_2 molecule, is related to the index of refraction μ and the number density n_s of scattering molecules by the Lorentz–Lorenz law,[49]

$$\gamma = (\tfrac{3}{4}\pi n_s)(\mu^2-1)(\mu^2+2)/(\mu^2+1) \approx (\mu-1)/2\pi n_s. \qquad (14)$$

[48] T. V. George, L. Goldstein, L. Slama, and M. Yokohama, Phys. Rev. **137**, A369 (1965).

[49] M. Born and E. Wolf, *Principles of Optics* (The MacMillan Company, New York, 1964), 2nd ed., p. 87.

PREIONIZER

MAIN COMPRESSION

CROWBAR

MAGNETIC FIELD

NEUTRON SIGNAL

5 μSEC/DIV.

MAGNETIC FIELD

LASER MONITOR

0.5 μSEC/DIV.

SIGNAL (0.2 V/DIV.)

MONITOR (0.05 V/DIV.)

0.5 μSEC/DIV.
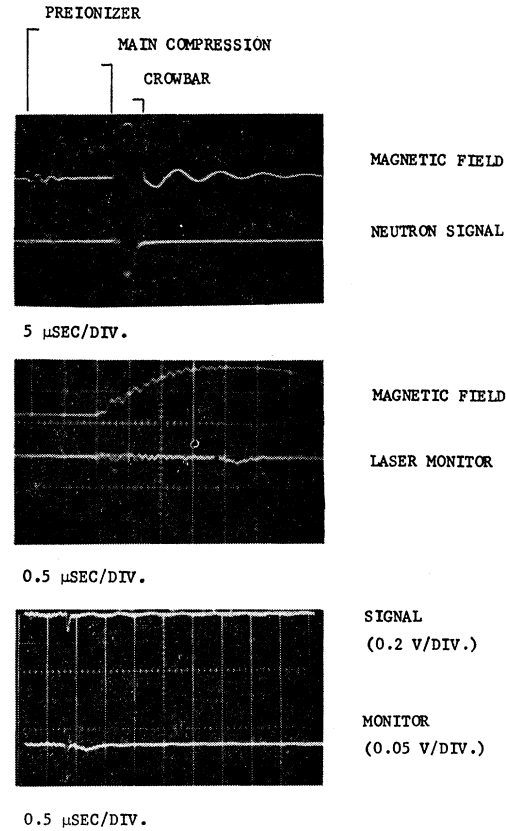
FIG. 6. Oscillograms typical of data from the scattering measurements.

Substituting $\mu - 1 = 2.967 \times 10^{-4}$ at STP, a scattered signal S corresponds to an absolute density–cross-section product of

$$n_s(d^2\sigma/d\Omega d\lambda)_R = 6.92 \times 10^{-12}(p\delta\lambda)(S/s)\,\mathrm{cm^{-1}/sr}\,\mathring{A}, \qquad (15)$$

where s is the Rayleigh-scattering signal measured at an N_2 pressure of p Torr, and $\delta\lambda$ is the spectral equivalent width of the spectrometer passband, measured as the FWHM of the stray-light or Rayleigh-scattered spectrum.

C. The Measured Spectra

Data were taken both with and without a small reverse bias magnetic field. Two independent runs with $B_0 = -750$ G yielded the results plotted in Fig. 7. The stray-light spectrum is also shown and has been subtracted from the scattered signals. A least-squares fit to a three-parameter Gaussian of the form $y = A\exp\{-[(\Delta\lambda + \Delta\lambda_0)^2/C^2]\}$ yields the following parameter values: $A = (1.68 \pm 0.09) \times 10^{-8}$ cm^{-1}/sr $\mathring{A}$, $C = 0.46 \pm 0.03$ $\mathring{A}$, and $\Delta\lambda_0 = 0.016 \pm 0.023$ $\mathring{A}$.

With no bias field (Fig. 8), the intensity of scattering was much smaller. The data in Fig. 8(a) were taken in a single run, and are fitted by a Gaussian with the following parameter values: $A = (4.81 \pm 0.24) \times 10^{-9}$ cm^{-1}/sr $\mathring{A}$, $\Delta\lambda_0 = -0.009 \pm 0.023$ $\mathring{A}$, and $C = 0.56 \pm 0.03$ $\mathring{A}$. Two more data runs with $B_0 = 0$ (and a different
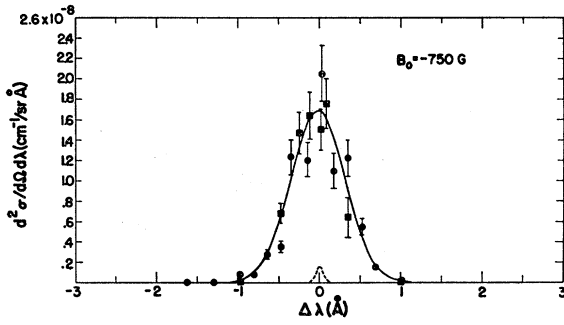
FIG. 7. Scattering results obtained with a bias field of -750 G. Two independent runs with separate absolute calibrations are shown by the squares and circles. The stray-light spectrum is shown by the narrow dashed curve.

discharge tube) are shown in Fig. 8(b). Here insufficient data were taken at small $\Delta\lambda$ to justify a three parameter fit, and $\Delta\lambda_0$ was set equal to zero. The other parameter values are $A = (6.63\pm0.34)\times10^{-9}\mathrm{cm^{-1}/sr}$ Å and $C = 0.51\pm0.04$ Å. The average maximum signal for the two Gaussian fits is 5.71×10^{-9} cm^{-1}/sr Å. Thus the scattered intensity for the plasma with $B_0 = -750$ G is 2.9 times larger than for the plasma with $B_0 = 0$.

The data of Fig. 8(b) were taken specifically to examine the wings of the spectrum, since it was ap-
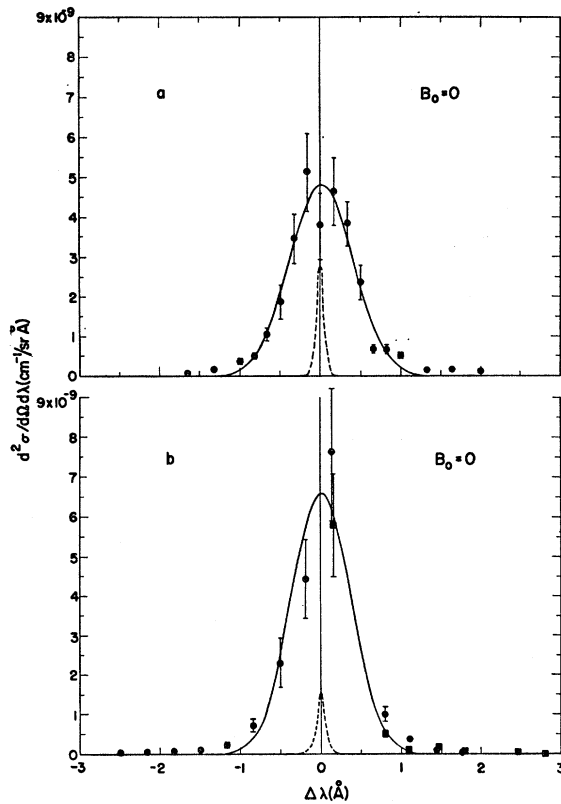
FIG. 8. Results of independent measurements with no bias field. In the lower graph the circles and squares represent independent runs.

parent from Fig. 8(a) that the wings of the first set of data were fitted only very poorly by the Gaussian curve. These later measurements, made in two runs, cover a range of three orders of magnitude of scattered signal, reaching down to the fluctuation level of bremsstrahlung. The results are replotted on a logarithmic scale in Fig. 9, along with the fitted Gaussian curve of Fig. 8(b). Also shown is a shaded band corresponding to the theoretical curve of Fig. 2 for $kT_i = 2$ keV. The flags of the data points represent the statistical variation of the scattered signals taken on different discharges, and the error band on the theoretical curve corresponds to the error in density quoted in Ref. 36. Variations in electron temperature are not expected to contribute as much to the error in the theoretical curve.

The principal results are: (a) that, within the experimental uncertainties, the wings of the scattered
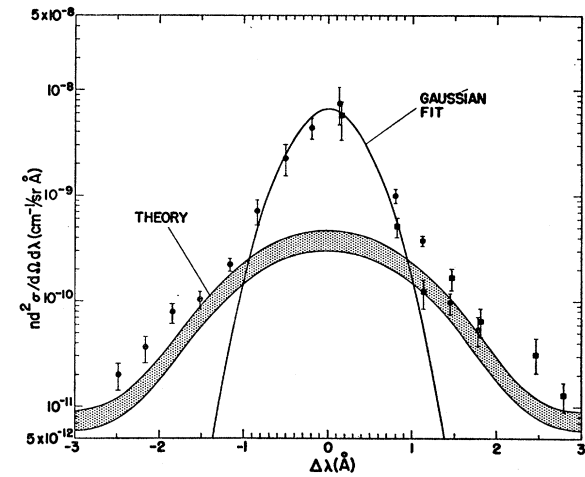
FIG. 9. Logarithmic plot of the data of Fig. 8(b). The solid curve is the Gaussian fit of Fig. 8(b), and the shaded band corresponds to the theoretical curve of Fig. 2 for $kT_i = 2$ keV, allowing for expected density variations.

spectrum for $B_0 = 0$ agree in magnitude and spectral width with the theoretically predicted scattering for a plasma with the known properties of the Scylla III plasma; (b) that the central part of the spectrum for $B_0 = 0$ has an intensity 15 times as great and a width only 0.44 as large as the theoretical prediction; and (c) when the plasma is produced with $B_0 = -750$ G the intensity of the central peak is increased by another factor of 3, while retaining approximately the same width.

V. DISCUSSION AND CONCLUSIONS

The data of Fig. 9 immediately suggest a model in which part of the scattering (the broad, low-intensity component) is due to thermal fluctuations, and part (the narrow, intense peak) is due to super-thermal density fluctuations which have an associated phase velocity 0.44 times the phase velocity of the thermal

fluctuations. This model is valid at least for the Fourier component ($|\delta\mathbf{k}| = 10^4$ cm^{-1}) observed in this experiment.

However, it is well to examine also the possibility that the narrow, intense spectrum is the result of thermal fluctuations and that the wide tail represents some other feature of the plasma-density fluctuations. The most cogent counterargument is that such an assumption would require a plasma density of 3.0×10^{17} cm^{-3}, as can be seen by comparing the narrow ion feature of Fig. 2 with the peak values of Fig. 8. This is in conflict with the measurement of the Scylla III density, $n = 2.8 \times 10^{16}$ cm^{-3}, referred to in Sec. IIIA, as well as with density measurements on other low-pressure, high-voltage θ pinches,[31-33] which show that n generally does not exceed about 3×10^{16} cm^{-3}. A second argument is that the broad tail corresponds both in magnitude and width to the expected thermal spectrum. Thirdly, the fact that a modest -750-G bias field increases the apparent intensity of the narrow central feature by a factor of 3 provides a qualitative indication that it is an artifice, not directly reflecting the bulk thermal properties of the plasma. We conclude, therefore, that it is the tail which represents the thermal density fluctuations.

It is interesting to estimate the magnitude of the anomalous diffusion across the magnetic field which might be caused by the plasma-density fluctuations corresponding to the central scattered peak. For $B_0 = 0$, the magnitude of these fluctuations is determined from the experiment by integrating the scattered intensity over wavelength: It is approximately $\frac{1}{2} \times 15 \times 0.44 = 3.3$ times as great as the magnitude of the thermal fluctuations, for the $|\delta\mathbf{k}| = 10^4$ cm^{-1} Fourier component. The factor $\frac{1}{2}$ accounts for the contribution of the electron feature which is approximately equal to that of the ion feature.

A rough estimate of the anomalous diffusion coefficient D produced by fluctuating electrostatic fields associated with small density fluctuations superimposed on a thermal plasma is given by the hydromagnetic theory for low-β plasmas[50,51]:

$$D = \epsilon(ckT_e/eB) = 16\epsilon D_B, \qquad (16)$$

where D_B is the Bohm diffusion coefficient, and ϵ is a Fourier sum over the mean-squared density fluctions,

[50] S. Yoshikawa and D. J. Rose, Phys. Fluids **5**, 334 (1962).
[51] B. B. Kadomtsev, J. Nucl. Energy Pt. C **5**, 31 (1963).

similar to those described by Eq. (10) for the thermal case:

$$\epsilon = (\tfrac{1}{4}\pi \sum_{\mathbf{k}} \langle |\delta n(\mathbf{k})|^2 \rangle / n^2. \qquad (17)$$

Having determined experimentally that the magnitude of superthermal scattering (for $\delta\mathbf{k} = 10^4$ cm^{-1}) is 3.3 times that of thermal scattering, we use Eq. (10) to give the density fluctuations corresponding to the superthermal component of the observed spectrum:

$$\langle |\delta n(\mathbf{k})|^2 \rangle / n^2 \approx 0.7 \times 33/N_e = 2.3/N_e, \qquad (18)$$

where the correlation factor corresponding to $(1+Z\alpha^2)/1+[Z+1]\alpha^2)$ of Eq. (10) has the value 0.7 for Scylla III conditions.[11] We make the crude approximation that the fluctuations are isotropic and that the mean-squared density fluctuation has this constant value for all k values up to the limit $2\pi/\lambda_D$ (beyond which collective motion no longer occurs), and is zero for higher k values. Then ϵ may be evaluated by the integral

$$\epsilon \approx (\pi/4) V(2\pi)^{-3} 4\pi \int_0^{2\pi/\lambda_D} dk\, k^2 (2.3/N_e) \approx 0.77\pi^2/n\lambda_D^3,$$
$$(19)$$

where V is the volume of the scattering electrons. Substituting the Scylla III parameter $\lambda_D = 0.83 \times 10^{-4}$ cm, we have $\epsilon = 0.5 \times 10^{-3}$, corresponding to an anomalous diffusion coefficient $D = 0.01 D_B$.

This estimate of D is of course very rough, since the assumed spectrum of density fluctuations may be quite unrealistic. The large k value singled out in the present experiment represents oscillations or instabilities of the plasma column (radius ≈ 1 cm) having wave mode numbers m of the order of thousands. On the other hand, the density fluctuations at small k and small m, which would more reasonably represent instabilities, may well be larger, corresponding to larger values of D. We are hopeful that further measurements, at different k values, will provide a reliable determination of the diffusion coefficient.

ACKNOWLEDGMENTS

FIG. 6. Oscillograms typical of data from the scattering measurements.